Objective Finite-Time Saddles and their Connection to FTLE

Roxana Bujack[1] Soumya Dutta[1] Irene Baeza Rojo[2] Duan Zhang[1] Tobias Günther[2]

[1]Los Alamos National Laboratory, United States
[2] Department of Computer Science, ETH Zürich, Switzerland

Abstract

Based on an intuitive physical definition of what a finite-time saddle-like behavior is, we derive a mathematical definition. We show that this definition builds the link between two FTLE-based saddle generalizations, which is not only of theoretical interest but also provides a more robust extraction of finite-time saddles.

CCS Concepts

• ***Human-centered computing*** → ***Scientific visualization;***

1. Introduction

Vector field topology [PC87a, HH89] is a common visualization method to analyze steady flow [PVH*03, LHZP07]. Critical points and separatrices segment the domain into coherent regions in which every streamline has the same origin and destination. It has been long known that instantaneous topology is not able to capture time-varying flow behavior [PT84]. Often two problems are named. First, time-varying data sets usually cannot be integrated infinitely long. Second, revealed features are not physically meaningful, which may refer to the fact that particles cross them. We think that integration to infinity would not be helpful when we want to analyze time-varying flow because the driving questions are usually related to finite-time phenomena, for example, from the time of the oil spill until now. This is why we emphasize our studies on the finite-time character of saddles. We strongly agree with the physically meaningful requirement and therefore only work with pathlines. Several great suggestions for a generalization to time dependent topology have been made, but none is considered a unified theory of finite-time topology yet [PPF*11].

In this paper, we are looking for a generalization of a saddle as known from classical vector field topology that is meaningful in a finite-time setting. To be meaningful, we expect the definition to at least satisfy the following three requirements:

- Detect steady saddles: We want the definition to detect the saddle in the vector field $(x,-y)^T e^{-\frac{x^2+y^2}{\sigma}}, \forall \sigma \in \mathbb{R}$ at $(0,0)^T$, which is the simplest, continuous, non-linear case that decays to zero velocity at infinite distance to the critical point.
- Objectivity: The definition should not depend on Euclidean transformations of the reference frame.
- Reflect movement of particles: The definition shall be pathline based and not streamline based.

For a basic and intuitive generalizaion, we start off with the idea of bifurcation lines [PC87b] or hyperbolic trajectories. Haller [Hal00] introduces uniformly hyperbolic trajectories in the context of Lagrangian coherent structures roughly speaking as pathlines with part of their neighboring pathlines converging in forward and part in backward direction. Later in [Hal11], he weakens the requirement to finite-time hyperbolicity, where a pathline does not need to satisfy hyperbolic behavior continuously but only overall for a given time interval. A fundamental difference between LCS and our work is that we do not require Lagrangianness. Instead of treating it an axoim, we consider it an open question whether or not a saddle will turn out to be a pathline in finite-time. Motivated by this, we use the following physical definition for a finite-time saddle, which forms a binary field in spacetime. For completeness, we also state its Lagrangian equivalent.

Definition 1 (Physical Definition of Finite-time Saddles) We consider a point and time $(x,t) \in \mathbb{R}^d \times \mathbb{R}$ a finite-time saddle for a given time interval $t \in (t_0,t_1)$ if part of its neighborhood has attracting behavior forward in time to t_1 and repelling behavior backward in time to t_0 while part of its neighborhood does the opposite.

Definition 2 (Physical Definition of Lagrangian Finite-time Saddles) We consider a pathline $x(t), x(t_0) = x_0$ a finite-time saddle for a given time interval $[t_0,t_1]$ if part of its neighborhood has attracting behavior and part of its neighborhood has repelling behavior forward in time from t_0 to t_1.

The two biggest contributions of this work are

- A mathematical definition for finite time saddles that matches the intuitive physical one and ties the link between Sadlo's FTLE-based saddles [SW10] and their Lagrangian counterpart.
- A measure for the detection of finite time saddles that does not depend on ridge detection or the error prone integration exactly on an unstable manifold [HY00].

DOI: 10.2312/evs.20191169

2. Related Work

In the 3D steady case, early work by Perry and Chong [PC87b] suggested that bifurcation lines are streamlines to which nearby streamlines are asymptotically drawn (or repelled away from) at an exponential rate.

Haller [HY00] used the term Lagrangian coherent structures (LCS) to refer to physically meaningful features in time-varying flow. He made use of the finite-time Lyapunov exponent (FTLE), which is a measure of separation of infinitesimally close particles over time. Recently, he summarized the past years of work on LCS, leading to a unified theory that gives hyperbolic, elliptic and parabolic LCS as lines that maximize attraction, repulsion, or shear in a certain time window [Hal15]. The extraction of LCS was discussed by Farazmand et al. [FH12] and the implementation details (and code) are given by Onu et al. [OHH15].

Theisel et al. [TWHS05] followed two approaches to the generalization of topology to unsteady vector fields. In their pathline-based approach, they categorized pathlines into attractors, repellors, and saddle-like trajectories based on whether their surrounding pathlines converge toward it in forward integration, in backward integration, or none of the above.

In their seminal work [SW10], Sadlo and Weiskopf generalized the concept of saddle-type critical points to time-dependent vector fields using the intersections of forward and backward FTLE ridges. They used these points as seeds for generalized streaklines as introduced by Wiebel et al. [WTS*07], which formed a generalization of separatrices to time-dependent flows. Üffinger et al. [USE13] extended the concept to 3D. Later, Üffinger [ÜSK*12] suggested to look at neighbor particles seeded on a circle around the reference particle and to replace the first-order separation approximation by the actual maximal separation among these particles.

Roth [Rot00] suggested to detect straight bifurcation lines by applying the parallel vectors operator of Peikert and Roth [PR99], namely by looking for places at which the velocity is parallel to the acceleration and at which all eigenvalues are real-valued. More recently, Machado et al. [MSE13, MBES16] applied the idea of Roth [Rot00] to locally detect bifurcation lines in 2D space-time. Since the method only works for saddles moving with equal speed in a constant direction, Machado et al. [MBES16] suggested to iteratively align the bifurcation line with a pathline of the flow. This method, however, cannot guarantee to find the correct solution.

3. Theory

In this section, we formulate a mathematical definition for finite-time saddles to match the physical definiton, cf. Def. 1. We analyze its mathematical properties, derive a first-order approximation, and demonstrate its relation to existing methods based on the intersection of forward and backward FTLE ridges.

3.1. Mathematical Definition

Definition 3 (Mathematical Definition of Finite-time Saddles) We consider a point and time (x_0,t) a finite-time saddle for a given time interval $t \in [t_0,t_1]$ if for any $\varepsilon > 0$, we can find 4 points $x_1,...,x_4 \in B_\varepsilon(x)$ in its ε-neighborhood (numbered in positive orientation around x) so that the pathlines starting at (x_1,t) and (x_3,t) will expand from x_0 forward in time until t_1 and contract backward until t_0 while (x_2,t) and (x_4,t) do the opposite.

We consider two trajectories $x_0(t),x_i(t) : \mathbb{R} \to \mathbb{R}^d$ expanding in forward time for a given finite time interval $t \in [t_0,t_1]$ if $\|x_0(t_0) - x_i(t_0)\| < \|x_0(t_1) - x_i(t_1)\|$ and contracting if $\|x_0(t_0) - x_i(t_0)\| > \|x_0(t_1) - x_i(t_1)\|$. Expansion in forward time is equivalent to contraction in backward time and vice versa.

So, with $F_t^{t_1}(x)$ being the flow map from time t to time t_1 of a particle seeded at x, we can equivalently require the conditions:

$$\begin{aligned} \|F_t^{t_1}(x_{odd}) - F_t^{t_1}(x_0)\| &> \|x_{odd} - x_0\|, \\ \|F_t^{t_1}(x_{even}) - F_t^{t_1}(x_0)\| &< \|x_{even} - x_0\|, \\ \|F_t^{t_0}(x_{odd}) - F_t^{t_0}(x_0)\| &< \|x_{odd} - x_0\|, \\ \|F_t^{t_0}(x_{even}) - F_t^{t_0}(x_0)\| &> \|x_{even} - x_0\|. \end{aligned} \tag{1}$$

This definition does not produce isolated points but areas. We can choose a point as representative, which we will call *saddle core*, for an area through demanding that it shows this behavior in locally the strongest way, like through locally maximizing

$$\begin{aligned} M_{t_0}^{t_1}(x_0,t) := \min\Big(&\frac{\|F_t^{t_1}(x_{odd}) - F_t^{t_1}(x_0)\|}{\|x_{odd} - x_0\|}, \frac{\|x_{even} - x_0\|}{\|F_t^{t_1}(x_{even}) - F_t^{t_1}(x_0)\|}, \\ &\frac{\|x_{odd} - x_0\|}{\|F_t^{t_0}(x_{odd}) - F_t^{t_0}(x_0)\|}, \frac{\|F_t^{t_0}(x_{even}) - F_t^{t_0}(x_0)\|}{\|x_{even} - x_0\|}\Big). \end{aligned} \tag{2}$$

Definition 3 is objective, i.e. invariant w.r.t Euclidean transformations of the reference frame $x' = Q(t)x + c(t)$ with a time-dependent orthogonal matrix $Q : \mathbb{R} \to SO(d)$ and translation $c : \mathbb{R} \to \mathbb{R}^d$, because it only depends on distances of particles at the same time.

3.2. Linear Approximation

Using Taylor's theorem, the difference between two close points can be expressed through the deformation gradient ∇F

$$F_t^{t_1}(x_0) - F_t^{t_1}(x_i) = \nabla F_t^{t_1}(x_0)(x_i - x_0) + O(\|x_i - x_0\|^2). \tag{3}$$

For the limit $\varepsilon \to 0$, we can write its magnitude as

$$\begin{aligned} \|F_t^{t_1}(x_0) - F_t^{t_1}(x_i)\|^2 &= (F_t^{t_1}(x_0) - F_t^{t_1}(x_i))^T (F_t^{t_1}(x_0) - F_t^{t_1}(x_i)) \\ &= (x_0 - x_i)^T (\nabla F_t^{t_1}(x_0))^T \nabla F_t^{t_1}(x_0)(x_0 - x_i). \end{aligned} \tag{4}$$

With $n = \frac{x_0 - x_i}{\|x_0 - x_i\|}$ and the Cauchy-Green strain tensor from continuum mechanics $C_{t_0}^{t_1}(x_0) = (\nabla F_{t_0}^{t_1}(x_0))^T \nabla F_{t_0}^{t_1}(x_0)$, we get

$$\frac{\|F_t^{t_1}(x_0) - F_t^{t_1}(x_i)\|^2}{\|x_0 - x_i\|^2} = n^T (\nabla F_t^{t_1}(x_0))^T \nabla F_t^{t_1}(x_i) n = n^T C_t^{t_1}(x_0) n, \tag{5}$$

which shows that the conditions in (1) can be expressed through the eigenvalues of C. In particular, the tensors $C_t^{t_1}(x_0)$ and $C_t^{t_0}(x_0)$ must each have eigenvalues greater as well as smaller than 1 so that point (x_0,t) is a first-order approximation to the finite-time saddle in the interval $[t_0,t_1]$.

The linear approximation is also objective. It follows

through direct calculation from the behavior of the deformation gradient under Euclidean transformations $\nabla {F_{t_0}^{t_1}}'(x') = Q(t_1)\nabla F_{t_0}^{t_1}(x)Q(t_0)^T$ [Liu03].

3.3. Relation to FTLE

Our measure is related to FTLE, where the largest eigenvalue λ_{max} of the Cauchy-Green strain tensor C is evaluated. To consider the dependence on the size of the time interval and the potentially rapid growth of the expansion, it is weighted via

$$FTLE_{t_0}^{t_1}(x_0) = \frac{\log\sqrt{\lambda_{max}(C_{t_0}^{t_1}(x_0))}}{t_1 - t_0}. \tag{6}$$

Analogously, we can weight the largest and smallest eigenvalue $\lambda_{max}, \lambda_{min}$ of the Cauchy-Green strain tensor for a weighted measure of strength

$$\tilde{M}_{t_0}^{t_1}(x_0,t) := \min\Big(\frac{\log\sqrt{\lambda_{max}(C_t^{t_1})}}{t_1 - t}, -\frac{\log\sqrt{\lambda_{min}(C_t^{t_1})}}{t_1 - t}, \frac{\log\sqrt{\lambda_{max}(C_t^{t_0})}}{t - t_0}, -\frac{\log\sqrt{\lambda_{min}(C_t^{t_0})}}{t - t_0}\Big)|v_{max}(C_t^{t_1})^T v_{min}(C_t^{t_0})|. \tag{7}$$

Scaling with the scalar product of the eigenvectors removes the case where they coincide, compare Figure 4. This shows that the intersection of forward $[t,t_1]$ and backward $[t,t_0]$ FTLE ridges over adjacent intervals at time t as suggested by Sadlo [SW10] is related to the two constraints in Definition 3 that correspond to the expansion. To see that the other two contracting criteria are important to reduce false positives, we take a look at the following example of a blue sky bifurcation, i.e. a sink that becomes a source. For $c \in [0,1)$ the vector field that has the shape $(-x,-cy)^T e^{-\frac{\sqrt{x^2+cy^2}}{\sigma}}$ if $t<0$ and $(-x,-cy)^T e^{-\frac{\sqrt{x^2+cy^2}}{\sigma}}$ if $t \geq 0$ has a ridge along the x-axis for $t<0$, which intersects the ridge along the y-axis for $t>0$ falsely indicating a saddle at the origin.

3.4. Lagrangian Invariance

Haller [Hal15] stated that the use of FTLE over sliding time windows produces non-Lagrangian results because the structures belong to different finite-time dynamical systems. This critique would also apply to the intersection of forward and backward FTLE ridges of adjacent time intervals as suggested by Sadlo and Weiskopf [SW10]. An adaption of their idea to a Lagrangian setting would suggest to look at the intersection of forward and backward FTLE ridges of the same interval instead, Figure 1. This ties back to the Lagrangian finite time saddles from Definition 2 because forward expansion equals backward contraction.

From condition (1) follows that the complete length of the pathline through $x(t) = x_0$ has overall saddle behavior, too, because of

$$\begin{aligned}\|F_t^{t_1}(x_{odd}) - F_t^{t_1}(x_0)\| > \|x_{odd} - x_0\| > \|F_t^{t_0}(x_{odd}) - F_t^{t_0}(x_0)\|,\\ \|F_t^{t_1}(x_{even}) - F_t^{t_1}(x_0)\| < \|x_{even} - x_0\| < \|F_t^{t_0}(x_{even}) - F_t^{t_0}(x_0)\|.\end{aligned} \tag{8}$$

The reverse is not true. For example, the flow that has the shape

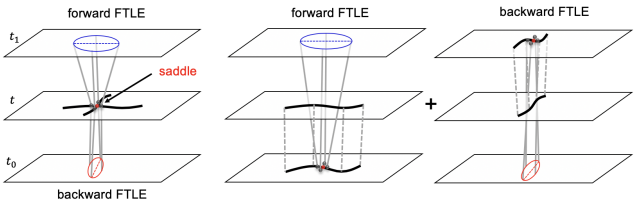

Figure 1: *The difference between adjacent interval ridges [SW10] (left) and same interval ridges [HY00] (middle + right).*

$(0,0)^T$ if $t<0$ and $(x,-y)^T e^{-\frac{\sqrt{x^2+y^2}}{\sigma}}$ if $t \geq 0$ would show saddle character for each pathline using the Lagrangian definition, while Definition 3, would only detect the parts of the pathlines that live in $t>0$. Also, the maxima in strength do not necessarily coincide with the maxima of the corresponding Lagrangian measure

$$\min\Big(\frac{\|F_t^{t_1}(x_{odd}) - F_t^{t_1}(x_0)\|}{\|F_t^{t_0}(x_{odd}) - F_t^{t_0}(x_0)\|}, \frac{\|F_t^{t_0}(x_{even}) - F_t^{t_0}(x_0)\|}{\|F_t^{t_1}(x_{even}) - F_t^{t_1}(x_0)\|}\Big), \tag{9}$$

or with the definition based on ridge intersection. However, every point (x_0,t) that is considered a saddle in Definition 3, lies on a pathline that has separating behavior for $[t_0,t_1]$ as well as backward for $[t_1,t_0]$, i.e., on one that can be considered a Lagrangian finite-time saddle. Nevertheless, it is possible that the saddle core line defined through the maxima $\text{argmax}(x,t)M_{t_0}^{t_1}(x,t)$ does not form a pathline.

This means that Definition 1 is sufficient but not necessary for Definition 2 for the pathline $x(t) = x$, but (2) not for (9).

3.5. Connection

The smallest forward FTLE $\mu_{t_0}^{t_1}(x_0)$ is the negative of the largest backward FTLE $\mu_{t_0}^{t_1}(x_0) = -\lambda_{t_1}^{t_0}((F_{t_0}^{t_1}(x_0))$ [HS11]. Now, through the basic Definition 3, we can see from (8) that the intersection of FTLE values over the same interval and over adjacent intervals are actually connected. Areas that have saddle behavior in the adjacent interval setting are areas of saddle behavior in the same interval setting if the demand for contracting behavior is added, Figure 1.

This connection provides a nice intuitive interpretation of the two methods that ties back to the expanding and compressing behavior of the classical steady saddle point.

This connection also solves a problem of the ridge intersection of the same interval setting. While for the adjacent intervals, the extracted ridges can readily be intersected in the time slice t, here, we would have to integrate the ridges to path surfaces whose intersection will then form the saddle pathline. This integration is highly unreliable because it is performed exactly on a repelling structure. In case of the experiment in Figure 2, the two surfaces do not even intersect at all. The ridges themselves do not suffer from that problem because at ridges only the fact that repulsion occurs is needed, not the exact form of the corresponding material surface. Using (9) can overcome that problem by a timestep-wise evaluation that only requires the information if repulsion takes place.

4. Experiments

We performed experiments on two analytical data sets, for which we know the ground truth, to demonstrate the correctness of

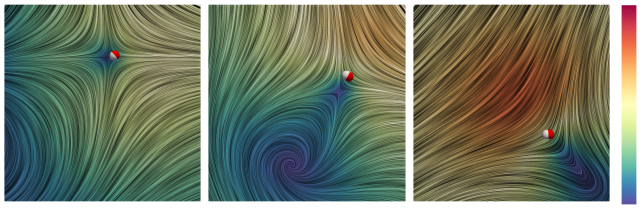

(a) *Saddle at t=2.* **(b)** *Saddle at t=4.* **(c)** *Saddle at t=6.*

Figure 2: *Detected saddle for accelerated translation. The white sphere shows the location detected by the proposed method and the red sphere shows the ground truth of the saddle location.*

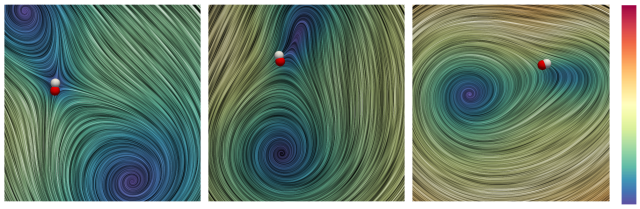

(a) *Saddle at t=2.* **(b)** *Saddle at t=4.* **(c)** *Saddle at t=6.*

Figure 3: *Results of detected saddle for accelerated rotation. The white sphere shows the location detected by the proposed method and the red sphere shows the ground truth of the saddle location.*

the proposed method. The first case is a steady saddle $v(x,y) = 20/|T|(x+0.5,-y)^T e^{-2\sqrt{(x+0.5)^2+y^2}}$ under an accelerated translation $v'(x,t) = v(x-c(t))+\dot{c}(t)$ by $c(t) = \frac{1}{2}(\sin(\theta)+1,\cos(\theta))^T$ with $\theta = 2\pi t^2/|T|^2$ and $|T|$ denoting the number of time steps. The saddle moves clockwise along the circle with radius 0.5 around $(0,0)$ starting at $(0,0.5)$. The second case is the same saddle under an accelerated rotation $v'(x,t) = Q(t)v(Q^T(t)x)+\dot{Q}(t)x$ with $Q(t) \in SO_2$ being the rotation matrix by $\theta = 2\pi t^2/|T|^2$. This saddle moves around the same circle starting at $(-0.5,0)$. We use the spatial domain $[-1,1]^2$ with resolution 41^2 and 10 time steps. Both transformations are purely Euclidean. They can be interpreted as a change of the reference frame of the observer and an objective method should be able to detect the saddle on the circle.

Figures 2 and 3 show the results of the detected locations of saddles on three selected time steps where the white sphere reflects the saddle location obtained by applying Definition 3. The line integral convolution (LIC) [CL93] visualization of the instantaneous vector field of the corresponding time step is displayed on the background as a context color coded by velocity magnitude. Note that the instantaneous LIC slice alone cannot reveal the motion of the saddle, since it shows streamlines instead of pathlines. The analytically computed correct saddle location is displayed using the red spheres. It can be observed that the saddle location detected by the proposed method conforms well with the ground truth, but the maximum always lies on a grid point, which is why the exact inner-cell location cannot be found.

The forward and backward FTLE as by Sadlo [SW10] produces the same results. Lagrangian forward and backward FTLE produces no result. The ridges are detected correctly at the first and last time step, but the path surfaces forward and backward along the highly unstable regions are deflected so strongly that they do not intersect at all in $[-1,1]^2$.

As a more complicated example, Figure 4 shows the quad gyre, which is the extension of the popular FTLE posterchild double gyre [SLM05] to the domain $[0,1]^2$ with resolution 201^2. Here, the global maximum saddle core line (yellow) of the Measure (7) coincides with the intersection of forward and backward FTLE of the adjacent intervals [SW10]. For comparison, we show the core line in cyan that was extracted using the parallel vectors operator as described by Machado [MSE13] without subsequent iterative pathline alignment, which is slightly off. Figure 4c shows the saddle core line detected with our method (yellow) in comparison to the one using the parallel vectors operator as described by Machado [MSE13]

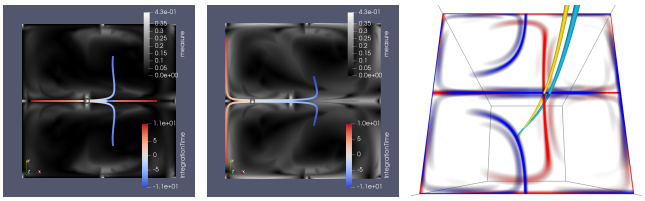

(a) *Measure (7) detects real saddle.* **(b)** *False positive without eigenvectors.* **(c)** *Our saddle core line in spacetime (yellow).*

Figure 4: *The strongest saddle detected with Measure (7) in the quad gyre coincides with the intersection of the forward an backward FTLE (red and blue in 4c).*

(cyan) on top of forward (red) and backward (blue) FTLE in spacetime. Pathlines seeded with offset in eigenvector direction in Figure 4b show how a temporary contraction with coinciding eigenvectors would produce a false positive if the weighting with the eigenvectors would be omitted in (7).

5. Discussion

We provided a definition for finite-time saddles that satisfies the requirements of steady saddle detection, objectivity, and particle movement reflection from the introduction. It does not demand Lagrangian invariance, but we could see that it produces a subset of the corresponding Lagrangian definition. The definition provides the flexibility that a particle can behave like a saddle for certain times without forcing it to either be a saddle or not for the whole time interval. Further, it provides the connection between, the intersection of forward and backward FTLE ridges for adjacent intervals and the Lagrangian version for the same interval. Finally, it motivates the computation of finite-time saddles without the necessity to extract ridges or the exact shape of a path surface in an unstable region, which makes it more robust.

We do not consider this the only or ultimate definition of objective finite time saddles because it still has some shortcomings. Same as FTLE, the integration duration must be chosen and the measure responds to shear, which is not desirable. Analogously to FTLE ridges, which become very thin for long integration times, the finite time saddle regions can become very small and and need high resolution. For complicated flows, the saddle-like regions can become very concave and are not as intuitive to interpret as their steady counterparts.

Acknowledgements

We gratefully acknowledge the support of the U.S. Department of Energy through the LANL Laboratory Directed Research Development Program under project number 20190143ER for this work published under LA-UR-19-21831.

References

[CL93] CABRAL B., LEEDOM L. C.: Imaging vector fields using line integral convolution. In *Proceedings of the 20th annual conference on Computer graphics and interactive techniques* (1993), SIGGRAPH '93, ACM, pp. 263–270. doi:10.1145/166117.166151. 4

[FH12] FARAZMAND M., HALLER G.: Computing Lagrangian coherent structures from their variational theory. *Chaos: An Interdisciplinary Journal of Nonlinear Science 22*, 1 (2012), 013128. 2

[Hal00] HALLER G.: Finding finite-time invariant manifolds in two-dimensional velocity fields. *Chaos: An Interdisciplinary Journal of Nonlinear Science 10*, 1 (2000), 99–108. 1

[Hal11] HALLER G.: A variational theory of hyperbolic Lagrangian coherent structures. *Physica D: Nonlinear Phenomena 240*, 7 (2011), 574–598. 1

[Hal15] HALLER G.: Lagrangian coherent structures. *Annual Review of Fluid Mechanics 47* (2015), 137–162. 2, 3

[HH89] HELMAN J., HESSELINK L.: Representation and display of vector field topology in fluid flow data sets. *Computer 22*, 8 (Aug 1989), 27–36. doi:10.1109/2.35197. 1

[HS11] HALLER G., SAPSIS T.: Lagrangian coherent structures and the smallest finite-time Lyapunov exponent. *Chaos: An Interdisciplinary Journal of Nonlinear Science 21*, 2 (2011), 023115. 3

[HY00] HALLER G., YUAN G.: Lagrangian coherent structures and mixing in two-dimensional turbulence. *Phys. D 147*, 3-4 (Dec. 2000), 352–370. URL: http://dx.doi.org/10.1016/S0167-2789(00)00142-1, doi:10.1016/S0167-2789(00)00142-1. 1, 2, 3

[LHZP07] LARAMEE R. S., HAUSER H., ZHAO L., POST F. H.: Topology-Based Flow Visualization, The State of the Art. In *Topology-based Methods in Visualization* (2007), pp. 1–19. doi:10.1007/978-3-540-70823-0_1. 1

[Liu03] LIU I.-S.: On the transformation property of the deformation gradient under a change of frame. *Journal of elasticity 71*, 1-3 (2003), 73–80. 3

[MBES16] MACHADO G., BOBLEST S., ERTL T., SADLO F.: Space-Time Bifurcation Lines for Extraction of 2D Lagrangian Coherent Structures. *Computer Graphics Forum 35*, 3 (2016), 91–100. URL: https://onlinelibrary.wiley.com/doi/abs/10.1111/cgf.12885, doi:10.1111/cgf.12885. 2

[MSE13] MACHADO G. M., SADLO F., ERTL T.: Local extraction of bifurcation lines. In *VMV* (2013), Citeseer, pp. 17–24. 2, 4

[OHH15] ONU K., HUHN F., HALLER G.: Lcs tool: A computational platform for lagrangian coherent structures. *Journal of Computational Science 7* (2015), 26–36. 2

[PC87a] PERRY A., CHONG M.: A description of eddying motions and flow patterns using critical-point concepts. *Annual Review of Fluid Mechanics 19*, 1 (1987), 125–155. 1

[PC87b] PERRY A. E., CHONG M. S.: A description of eddying motions and flow patterns using critical-point concepts. *Annual Review of Fluid Mechanics 19*, 1 (1987), 125–155. doi:10.1146/annurev.fl.19.010187.001013. 1, 2

[PPF*11] POBITZER A., PEIKERT R., FUCHS R., SCHINDLER B., KUHN A., THEISEL H., MATKOVIC K., HAUSER H.: The State of the Art in Topology-based Visualization of Unsteady Flow. *Computer Graphics Forum 30*, 6 (September 2011), 1789–1811. URL: http://dx.doi.org/10.1111/j.1467-8659.2011.01901.x. 1

[PR99] PEIKERT R., ROTH M.: The parallel vectors operator: A vector field visualization primitive. In *Proceedings of the Conference on Visualization '99: Celebrating Ten Years* (Los Alamitos, CA, USA, 1999), VIS '99, IEEE Computer Society Press, pp. 263–270. URL: http://dl.acm.org/citation.cfm?id=319351.319420. 2

[PT84] PERRY A., TAN D.: Simple three-dimensional vortex motions in coflowing jets and wakes. *Journal of Fluid Mechanics 141* (1984), 197–231. 1

[PVH*03] POST F. H., VROLIJK B., HAUSER H., LARAMEE R. S., DOLEISCH H.: The State of the Art in Flow Visualisation: Feature Extraction and Tracking. *Computer Graphics Forum 22*, 4 (2003), 775–792. URL: http://dx.doi.org/10.1111/j.1467-8659.2003.00723.x, doi:10.1111/j.1467-8659.2003.00723.x. 1

[Rot00] ROTH M.: *Automatic extraction of vortex core lines and other line type features for scientific visualization*, vol. 2. Hartung-Gorre, 2000. 2

[SLM05] SHADDEN S. C., LEKIEN F., MARSDEN J. E.: Definition and properties of Lagrangian coherent structures from finite-time Lyapunov exponents in two-dimensional aperiodic flows. *Physica D: Nonlinear Phenomena 212*, 3 (2005), 271–304. 4

[SW10] SADLO F., WEISKOPF D.: Time-dependent 2-d vector field topology: An approach inspired by lagrangian coherent structures. In *Computer Graphics Forum* (2010), vol. 29, Wiley Online Library, pp. 88–100. 1, 2, 3, 4

[TWHS05] THEISEL H., WEINKAUF T., HEGE H.-C., SEIDEL H.-P.: Topological methods for 2D time-dependent vector fields based on stream lines and path lines. *Visualization and Computer Graphics, IEEE Transactions on 11*, 4 (July 2005), 383–394. doi:10.1109/TVCG.2005.68. 2

[USE13] UFFINGER M., SADLO F., ERTL T.: A Time-Dependent Vector Field Topology Based on Streak Surfaces. *IEEE Transactions on Visualization and Computer Graphics 19*, 3 (March 2013), 379–392. doi:10.1109/TVCG.2012.131. 2

[ÜSK*12] ÜFFINGER M., SADLO F., KIRBY M., HANSEN C. D., ERTL T.: FTLE Computation Beyond First-Order Approximation. In *Eurographics (Short Papers)* (2012), pp. 61–64. 2

[WTS*07] WIEBEL A., TRICOCHE X., SCHNEIDER D., JAENICKE H., SCHEUERMANN G.: Generalized streak lines: Analysis and visualization of boundary induced vortices. *IEEE Transactions on Visualization and Computer Graphics 13*, 6 (2007), 1735–1742. 2